

Low-Energy Electron Damage to Condensed-Phase Deoxyribose Analogues Investigated by Electron Stimulated Desorption of H^- and Electron Energy Loss Spectroscopy

D. Antic,* L. Parenteau, M. Lepage, and L. Sanche

Groupe du Conseil de Recherches Médicales du Canada en Sciences des Radiations, Faculté de Médecine, Université de Sherbrooke, Québec, J1H 5N4, Canada

Received: February 25, 1999; In Final Form: May 3, 1999

We report the 5–20 eV electron-stimulated desorption (ESD) yields of H^- produced by dissociative electron attachment (DEA) to the DNA backbone sugar-like analogues tetrahydrofuran (**I**), 3-hydroxytetrahydrofuran (**II**), and α -tetrahydrofurfuryl alcohol (**III**) physisorbed on a polycrystalline Pt substrate. For the pure disordered solid films, we observe one peak in the H^- yield function at an incident electron energy, E_i , of ~ 10 eV, which is attributed to selective dissociation of endocyclic α -CH bonds via the formation of a core-excited shape resonance; no desorbing polyatomic fragments were detected. A second peak is also observed in the H^- ESD yield function of **II**; it appears as a weak shoulder superimposed on the low-energy side of the 10 eV structure displaying a sharp vertical onset near 6.7 eV and a peak maximum around 7.3 eV. The sharp onset and narrow energy width are characteristic of a core-excited Feshbach resonance; it is attributed to H^- produced via DEA to the OH substituent whose corresponding parent state may be similar to that observed in CH_3OH , where the 7.3 eV resonance originating from the hydroxyl group was assigned to a $2\text{A}''$ Feshbach resonance. High-resolution electron energy loss (HREEL) spectra recorded with 11 and 14 eV incident electrons are also reported for solid **I**. They show that, with increasing electron dose, degradation of the solid leads to formation of a C–O π -bonded product believed to arise from fragmentation of an α -cleaved transient intermediate following direct electronic excitation of the parent molecule. The HREEL spectra suggest a rather complex fragmentation pathway following low-energy electron bombardment. In vacuo kinetic energy (E_k) distribution measurements of desorbed H^- in the 10 eV resonance suggest that for **I**, **II**, and **III** a dissociation mechanism similar to that proposed for the 14 eV HREELS spectra occurs, whereby α -cleavage of the C–O bond occurs within the lifetime of the dissociative negative ion state.

I. Introduction

Chemical and physical processes stimulated at surfaces or within solids by low-energy electrons (< 20 eV) play important roles in a variety of contexts. These include the aging and dielectric breakdown of insulators,^{1,2} structural modifications of self-assembled monolayers,^{3,4} chemical modification of Si ,^{5,6} and fabrication of nanostructures via scanning tunneling microscopy (STM).⁷ Furthermore, the energy selectivity, large cross-sections,^{8–10} and sensitivity to molecular environment^{11,12} of very specific electron-induced resonant reactions (such as dissociative electron attachment, DEA) indicate their potential usefulness in the rapidly growing field of tunable chemistry at surfaces.

Thus, it is not at all surprising that low-energy electron reactions also represent an important element in the radiation sciences,^{13,14} particularly the early sequence of events immediately following the interaction of ionizing radiation with biological media. It is well-known that when such radiation deposits its energy in a cell, it produces copious amounts of low-energy secondary electrons, the majority of which are created along the radiation tracks with initial kinetic energies well below 20 eV.^{15–18} At these energies, electrons are known to induce production of anion and neutral fragments from small molecules,^{19–21} including physisorbed linear²² and cyclic hydrocarbons,^{23,24} as well as chemisorbed hydrocarbons.^{3,25} Recent

work on biological molecules has included DEA to DNA bases,^{26,27} radiosensitizing 5-halouracils and homo-oligonucleotides.²⁵ These studies have shown that resonant electron attachment leads to formation of a multitude of different anion species from gas-phase thymine or cytosine²⁶ and condensed-phase 5-Br-uracil.^{27,28}

In the present survey study, we have investigated DEA to physisorbed tetrahydrofuran (**I**), 3-hydroxytetrahydrofuran (**II**), and α -tetrahydrofurfuryl alcohol (**III**) whose molecular structure is shown in Figure 1a. These molecules are of particular interest to our current research on low-energy electron damage to organic/biological solids, since some of their basic molecular features (structure or functional groups) approximate those found in the deoxyribose backbone of DNA [Figure 1b], thus serving as model compounds to qualitatively estimate the relative effects of DEA in these specific DNA sites. To date, no results have been reported on the chemical consequences of the interaction of secondary electrons of low energies with the deoxyribose backbone of DNA and its constituents. Such work has been essentially concentrated on chemical or biological damage induced by thermalized electrons. Even in the latter case, only a few studies have stressed the importance of thermal electron attack on sugar molecules along the DNA backbone,^{29–31} since most investigations have focused on migration along the DNA base π -stack and subsequent localization on its pyrimidine bases^{32–36}

Previous degradation studies of the presently investigated compounds have been mainly concerned with photochemical

* To whom correspondence should be addressed.. E-mail: dean.antic@sympatico.ca. Fax: (819) 564-5442.

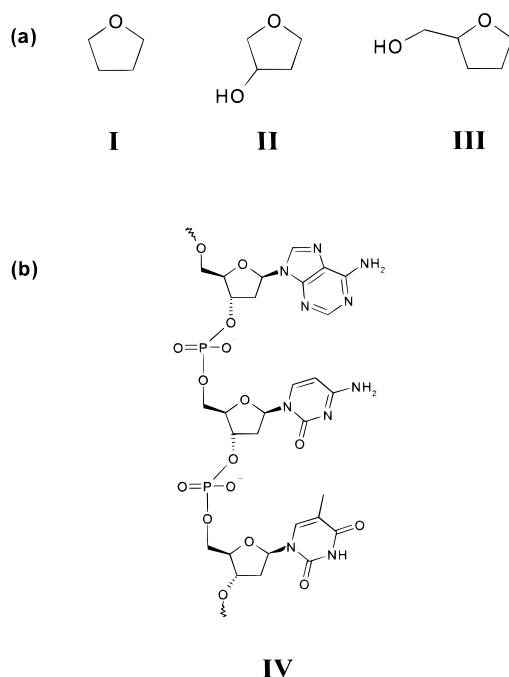


Figure 1. Schematic drawing of (a) the DNA backbone sugar-like analogues tetrahydrofuran (**I**), 3-hydroxytetrahydrofuran (**II**), and α -tetrahydrofurfuryl alcohol (**III**), and (b) a short-chain segment of a single-stranded deoxyribose backbone of DNA.

studies^{37–44} of the ring cleavage dynamics of **I** in the gas,^{37,38,42–44} liquid,^{40,41} and solid phases.⁴³ Photon-induced excitation of the parent (**I**) results in the formation of an oxyl alkyl diradical ($\cdot\text{CH}_2\text{—CH}_2\text{—CH}_2\text{—CH}_2\text{—O}\cdot$) following homolytic cleavage of the C—O bond. Scala and co-workers⁴⁴ have studied the β -cleavage dynamics of **I** on the femtosecond time scale using 307 nm photons and found that β -elimination involving the C—H bond is a major channel in the fragmentation pathway of the diradical intermediate and leads to C—C and C—O π bond formation. However, only a few studies of DEA to related compounds, such as furan, lactams, and related five-member heterocyclic compounds,^{45–48} exist, and only in the gas phase, and to the best of our knowledge, no previous data have been reported on either condensed- or gas-phase DEA to **I**, **II**, or similar deoxyribose analogues. It should, however, be noted that considerable computational^{30,49–51} and UV photoelectron studies⁵⁰ have been reported on deoxyribose radicals, radical cations, and structurally related compounds, with an emphasis on radical stability, charge localization, and transfer following DNA irradiation.

Experimental data on the electronic states and electron energy loss (EEL) are limited for **I** and appear to be nonexistent for **II** and **III**. Near-threshold gas-phase EEL spectra for **I** reveal three broad, low-lying absorption bands.⁵² These bands are assigned to excitation of Rydberg states 1n_03s , 1n_03p , 1n_03d with maxima near 6.6, 7.2, and 7.8 eV, respectively,^{52,53} and agree well with vacuum ultraviolet (VUV) spectra.^{52,54–56} It has been suggested⁵² that the origin of the first excited state may also contain a valence excitation and, in addition, may support a negative ion resonance. Measurements of excitation functions of several vibrational energy loss channels in solid **I** reveal selective vibrational enhancements and have been assigned to nondissociative σ^* shape resonances located near 4, 7.5, and 10 eV, with possible contributions from overlapping core-excited resonances at higher impact energies.⁵⁷ At impact energies of ≥ 8 eV, the gas-phase EEL spectrum⁵² shows a broad continuous absorption with little fine structure up to the first ionization

threshold near 9.79 eV.^{50,52} Comparison of EEL spectra with VUV spectra reveals three additional Rydberg states converging to the first ionization limit: 1n_04p (8.57 eV), 1n_05p (8.89), and 1n_03s (HOMO-1 $\rightarrow 3s$; ~ 8.1 eV). Consequently, the higher-lying resonances are believed to arise from contributions from several overlapping core-excited parent states.⁵⁷

In the present contribution, we report measurements of H^- electron-stimulated desorption (ESD) yields and H^- kinetic energy (KE) distributions from physisorbed solids of **I**, **II**, and **III**, as well as high-resolution electron energy loss (HREEL) spectra from **I**. Our H^- yield measurements show that resonant electron attachment to such deoxyribose derivatives leads to DEA not only via ring CH bond cleavage but also possibly via dissociation of exocyclic OH and CH bonds. In this case, for at least **I**, the 10 eV peak in the H^- ESD yields is attributed to a dissociative core-excited shape resonance, where the molecular negative ion state (NIS) lies above the energy of the neutral excited parent state. DEA-induced dissociation to the hydroxyl O—H bond in **II** via a core-excited Feshbach resonance is also found to contribute to the H^- yield at lower energies, whereas in **III** this same resonance is not apparent. Finally, our HREEL measurements of condensed phase **I** show that (a) at electron energies between 6 and 9.5 eV, there exist several overlapping electronically excited states and (b) degradation of the solid **I** by electrons of energies within the range 11–14 eV leads to formation of possibly three different C—O π -bonded aldehyde type fragments, which are most likely formed after electron radical autodetachment from the NIS, via the fragmentation of a ring-opened intermediate.

II. Experimental Methods

The apparatus, operating modes, and experimental methods used in the ESD measurements have been described in considerable detail elsewhere.^{12,22,58,59} Briefly, multilayer films of **I**, **II**, and **III** are grown in a vacuum on an electrically isolated polycrystalline platinum ribbon attached to the tip of a closed-cycle helium-refrigerated cryostat. The Pt ribbon is cleaned by resistive heating to ~ 800 °C. A collimated 4–5 nA incident electron beam emanating from a hemispherical monochromator with a full width at half-maximum (fwhm) beam resolution of ~ 80 meV impinges onto the target film at an incident angle of 70° from the surface normal. The incident electron beam energy E_i is calibrated to within ± 0.15 eV of the vacuum level by measuring the onset of current transmission into the multilayer film.⁶⁰ A fraction of the negative ion flux desorbing from the surface during electron impact is collected at an angle of 20° at the opposite azimuth. The desorbed anions are focused into a quadrupole mass spectrometer (QMS) by electrostatic lenses. All components are housed in an ultrahigh vacuum (UHV) system reaching a base pressure of $\sim 2 \times 10^{-10}$ Torr.

There are two modes of operation for the ESD apparatus.⁵⁸ In the ion yield mode, negative ions are mass-selected and the yield of desorbing anions are measured as a function of E_i , while the retardation voltage V_r on a pair of grids positioned directly in front of the QMS is set to transmit anions of all energies. In the ion energy mode, the mass selection of the QMS and E_i is held fixed and the anion signal intensity is monitored as a function of V_r over a suitable range. The resulting retardation curves, which define the anion KE (E_k), are smoothed using a fast Fourier transform or an adjacent averaging smoothing algorithm in order to reduce the noise level in the raw data. Upon taking the negative derivative of the smoothed curves with respect to V_r , anion E_k distributions are obtained. Oscillations due to the noise level in the raw data become strongly amplified

upon differentiation, and therefore, all KE distribution curves presented here for H^- have been obtained after smoothing of the raw data. The shape and position of the E_k distributions have been shown⁵⁸ to remain unchanged upon minor variation of parameters in the smoothing algorithms.

From the E_k distributions, the experimental quantities of interest in the present study that may be obtained are the most probable kinetic energy $E_k(\text{mp})$ and the maximum observable kinetic energy $E_k(\text{max})$. The $E_k(\text{mp})$ is defined as the energy position of the peak in the distribution and is obtained, typically, by a Gaussian fit of the distribution function. Alternatively, $E_k(\text{mp})$ can be obtained by visual inspection of the E_k distribution, though the former method proves to be more rigorous and also more useful when multiple peaks are present in the E_k distributions. The $E_k(\text{max})$ is defined as those anions that desorb into vacuum following minimal inelastic losses. In the present study $E_k(\text{max})$ was defined directly from the retardation curves as that V_r for which the H^- signal has been reduced to $\sim 1\%$ of the unretarded intensity.

HREEL spectra of condensed films of **I** were measured at an incident angle of 10° from the normal and a fixed collection angle of 45° . Vibrational and electronic losses of **I** were recorded from threshold up to an incident energy E_i of 11 and 14 eV. The electron spectrometer used for these measurements is a modified version of the one previously described.⁶¹ The spectrometer consists of a hemispherical electrostatic deflection monochromator and analyzer. The incident and scattered electrons are focused using a set of double zoom lenses attached to the exit and entrance of the monochromator and analyzer, respectively. The monochromator can be rotated between 8° to 80° from the surface normal, and the analyzer is fixed at 45° at the opposite azimuth. The incident electron current is of the order of 0.1 nA with a nominal system beam resolution of 11 meV (fwhm). The incident electron energy E_i is calibrated to within ± 0.1 eV of the vacuum level by measuring the onset of current transmitted through the multilayer film.⁶⁰ Samples are deposited on a Pt(111) single crystal that is connected to the cold end of a closed-cycle helium-refrigerated cryostat and is attached to (but electrically and thermally isolated from) an XYZ manipulator that is also capable of azimuthal and flip rotations, as described previously.⁶² All components are housed in a bakeable UHV system; the spectrometer is operated at a pressure of 6×10^{-11} Torr.

In the present ESD study, 10 monolayer (ML) thick films of **I**, **II**, and **III** [Figure 1a] were grown on the platinum substrate held at a temperature of ~ 27 K. The samples were prepared in a gas-handling manifold and condensed onto the substrate from the vapor phase. During deposition, the condensing sample vapors were analyzed for impurities by a residual gas analyzer. The film thickness was determined, as previously described,⁶³ by a gas volume expansion method with an uncertainty of $\pm 50\%$ and a reproducibility of 5–10%. Samples of **I** (99.9+%), **II** (99%), and **III** (99%) were purchased from Aldrich and introduced in the manifold at the stated purity, where they were subjected to several in situ degassing cycles prior to deposition. Contamination from water is less than 0.005% in **I** and less than 0.02% in **II** and **III**. HREEL spectra of **I** were measured on 10 and 16 ML thick films prepared in the same manner.

III. Results and Discussion

A. ESD from Pure Films of I, II, and III. Figure 2 shows the H^- ion ESD yields measured for $0 \leq E_i \leq 20$ eV from 10 ML films of **I**, **II**, and **III**. The curves in Figure 2 are characterized by an onset in the H^- yield at 6.0, 5.8, and 6.0

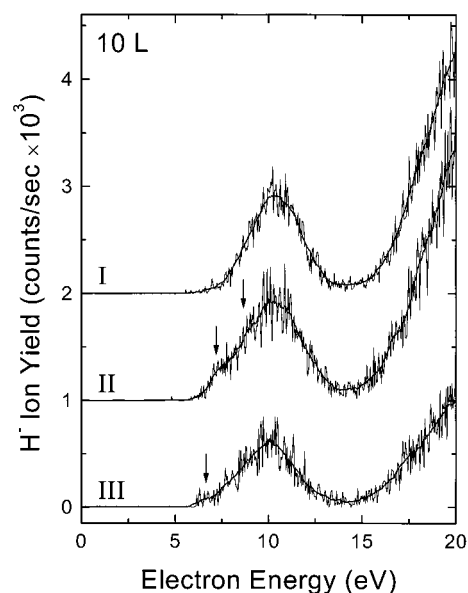
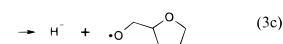
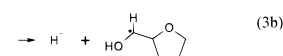
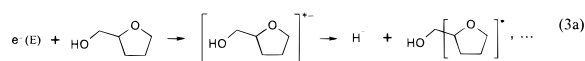
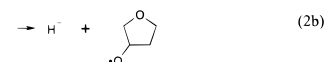
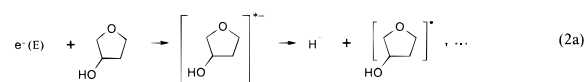
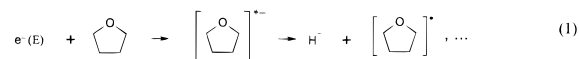


Figure 2. H^- desorption yields stimulated by the impact of 0–20 eV electrons on a 10 monolayer (ML) thick film of **I**, **II**, and **III**. In this figure, the small arrows indicate the positions of the two Feshbach resonances associated with DEA to the hydroxyl group in **II** and **III**, respectively. The smooth solid lines serve as guides to the eye, and the curve baselines have been shifted vertically for clarity.

SCHEME 1



eV and a yield maximum centered at 10.4, 10.2, and 10.0 eV for **I**, **II**, and **III**, respectively. The fwhm of the 10 eV structure was determined to be 3.3, 3.8, and 3.6 eV for **I**, **II**, and **III**, respectively, by fitting a Gaussian function to the experimental curves. A second feature is also observed in the H^- yield function for **II**; it appears as shoulder on the low-energy side of the 10 eV peak and is characterized by a sharp onset and a peak maximum near 7.3 eV. All features below 15 eV are characteristic of DEA to physisorbed molecules. The steep rise in the H^- signal with an energetic threshold near 14.5 eV is characteristic of nonresonant dipolar dissociation (DD) of C–H bonds²² in **I**, **II**, and **III**; it could also partially arise from DD of the O–H bond in **II** and **III**. DD to condensed-phase **I**, **II**, and **III** will be discussed in detail in a forthcoming publication.⁶⁴

For **I**, **II**, and **III**, the formation of H^- via DEA may be written explicitly to proceed via the reactions shown in Scheme 1. Other decay channels of the NIS (not shown), which may result in the formation of larger anion fragments, such as the OH^- , CH_2OH^- , and the $(M - 1)^-$ ion fragment, may also

compete with H^- production, but, as shall be discussed below, these larger mass fragments typically do not possess sufficient KE to escape the polarization energy (E_p) and thus remain trapped within the film.

For reactions 1–3 to be completed, several conditions must be met: (a) the NIS must be dissociative in the Franck–Condon region of the ground-state neutral molecule; (b) the resonance's electron autodetachment lifetime, $\tau_a = \{\hbar/\Gamma_a\}$, where Γ_a is the uncertainty width of the NIS, must be similar to or longer than one vibrational period of the nuclei (i.e., $\sim 10^{-14}$ s); (c) the electron affinity of the fragment carrying the negative charge must be positive. If, on the other hand, the lifetime of the molecular anion state is significantly less than one vibrational period, then the resonant electron will autodetach, leaving the molecule in the ground state or excited states.

By comparison to **I**, we note that there is only a slight modification in the 10 eV peak position, that is, a successive downward shift of 0.2 eV upon substitution of a ring hydrogen with an $-OH$ or $-CH_2OH$ group, respectively. The maximum intensity of the 10 eV peak in **I** and **II** remains, however, nearly identical upon substitution of the hydroxyl group at the β -carbon position. In contrast, the H^- desorption yield maximum is found to decrease by $\sim 35\%$ for **III** despite the 33% increase in the total amount of hydrogen upon substitution of a ring hydrogen with a CH_2OH group. Similarly, the peak width of the 10 eV feature remains essentially constant for **II** and **III**, with a slight increase of ~ 0.3 eV relative to **I**. These observations suggest that for DEA to **I–III**, the initial formation of the NIS is essentially *localized* on the heterocyclic ring, most likely occurring exclusively at the α -carbon position, and that DEA, which may occur in either of the exocyclic OH or CH_2OH groups, does not compete significantly to the depletion of the observed 10 eV H^- signal. Indeed, the decrease in the H^- ESD yield in **III** is attributed solely to the replacement of an α -H in the heterocyclic ring, where the decrease in signal is commensurate with the decrease in the number of α hydrogen atoms.

In general, the DEA H^- yields observed here are similar to those measured from other condensed cyclic hydrocarbons, e.g., aniline,²⁴ other benzene derivatives including pyrimidine,²³ as well as linear saturated and unsaturated hydrocarbons.²² However, in the case of aniline and pyrimidine the addition of an amino group in the former or substitution of two nitrogen atoms in the benzene ring in the latter results in a substantial reduction in the H^- desorption yield in comparison to benzene. Furthermore, in aniline, the presence of the amino group leads to formation of at least one additional DEA resonance below the one responsible for the observed H^- ESD yield from the phenyl group and also effectively competes with electron attachment to the benzene ring. Clearly, this is not the case for the derivatives of **I**. Owing to the strong similarity of the H^- desorption profiles, we conclude that *the majority of the anion yield for all three systems studied arises from at least one electron resonance associated with electron attachment to the furan ring*.

Selective dissociation of the α -CH bonds can be rationalized by considering rather straightforward arguments regarding the relative stability of the resulting neutral products; the initial formation of the radical site is determined in large part by the bond strength of the dissociating bond, which in turn is determined by both the ability of attached or neighboring groups to stabilize the unpaired electron via delocalization and the structural changes at the radical center.

Formation of a radical site at either of the two α -carbon positions following bond cleavage of any one of the four (**I**

and **II**) or three (**III**) α -CH bonds is expected to be favored over β -carbon-centered radicals owing to the directly attached oxygen heteroatom. This difference in reactivity is reflected in the bond dissociation energy where, for unsubstituted **I**, the α -CH bond strength is approximately 4 eV⁶⁵ versus a slightly higher value of 4.12 eV for the β -CH bonds.⁶⁶ In recent ab initio Hartree–Fock^{29,51} and MP2⁵¹ level studies on deoxyribose-centered radicals,⁶⁷ the stability of the radical site was found to depend to a large degree on the flexibility of the ring to accommodate the unpaired electron. Moreover, the stability of the substituted α -carbon-centered radicals was found to be nearly equal, followed closely by the unsubstituted and substituted β -carbon radicals, respectively. The order of radical site stability was rationalized on the basis of arguments of geometrical changes in the deoxyribose ring upon radical formation, where in the former larger changes in the pseudorotation phase angle were found. Furthermore, the initial excitation by the resonant electron, prior to electron capture, is most probably that of an oxygen lone pair electron. Transfer of an electron from a strongly electronegative atom to a nonbonding Rydberg orbital will result in a flow of electrons in order to compensate the loss, which leads to a weakening of neighboring bonds. Therefore, we should expect to see selective dissociation at the α -carbon position in both the unsubstituted (**I** and **II**) and substituted (**III**) molecules with little contribution from β -CH bond cleavage. This is clearly the case in the present study. Consider, for example, **II** resulting from substitution of a β -H in **I** with an OH group. In this case the observed H^- desorption yield remains unchanged. However, upon substitution of an α -H in **I** with a CH_2OH group, the H^- intensity in **III** decreases by $\sim 35\%$ (the integrated H^- yield decreases by $\sim 30\%$), which is nearly proportional to the total change in the number of α -hydrogen atoms.

From the H^- ESD desorption yields in Figure 2 it is evident that at least one electron resonance is responsible for the formation of H^- at 10 eV. Owing to the largely Rydberg character of the excited states in **I** (see below) near the energy range of the observed resonance, we suggest that this resonant state is of the core-excited type, possibly with dissociative valence σ^* configurational mixing. Lepage et al.⁵⁷ have observed a broad resonance at similar electron energies in the excitation function of several vibrational modes in **I**, where they found good correlation with the gas-phase resonance observed in cyclopentane,⁶⁸ and have tentatively assigned it as a core-excited shape resonance. This assignment is consistent with that made for the resonance observed near 10 eV for the $(M - 1)^-$ fragment (as well as all the lower mass fragments) produced in DEA to gaseous furan.⁴⁵ In a core-excited shape resonance, electron capture is accompanied by electronic excitation. The nature of the excited state can be of Rydberg or valence character, but the energy of the resonance generally lies above the parent state. Thus, on the basis of comparisons to photoelectron spectra of furan, Muftakhov et al.⁴⁵ assigned the 9.8 eV core-excited shape resonance as arising from excitation of an electron from a lower-lying $\pi(b_1)$ molecular orbital associated with electron capture in a diffuse symmetric quasi-Rydberg type molecular orbital, in effect producing a cationic species similar to that obtained in UV photoelectron experiments except with two nonbonding Rydberg electrons attached.⁶⁹ Hence, by analogy, we may infer, on the basis of a comparison to photoelectron spectra⁵⁰ of **I**, that, in the 10 eV resonance, electron promotion occurs from a similar molecular orbital but of σ - or n -type, with a corresponding ionization potential in the range 12–13 eV and resonant electron capture in an ns or

np Rydberg-type orbital. These Rydberg-type excitations are well-known^{70,71} in saturated oxo compounds, and their excitation spectra are typically dominated by them. As such, we may envisage the initial excitation as arising from an oxygen 2p orbital, probably the HOMO-1, resulting in an $^{1,3}n_{\text{O}}n_{\text{s}}$ or $^{1,3}n_{\text{O}}np$ excited state, where the principal quantum n is either 3 or 4. These states have been observed in VUV^{52,54–56} spectra and the gas-phase⁵² and the present electron energy loss spectra of **I**, though in the last two are found to be more diffuse and shifted to higher energies. However, these states appear in the range $6.2 \leq E_i \leq 8.9$ eV, i.e., at too low energies to be associated with the formation of a core-excited resonance that can account for the H^- ESD peak observed near 10 eV. Therefore, we are led to the conclusion that since the parent electronic state must lie above the lower Rydberg series, the initial electronic excitation must indeed arise from a deeper lying molecular orbital, possibly of σ -type.

The lower energy structure that appears near $E_i = 7.3$ eV for **II** in Figure 2 is clearly absent in the H^- yield curve of **I** and can therefore be associated with DEA to the endocyclic hydroxyl group [Scheme 1, reaction 2b] and tentatively attributed to a low-lying core-excited resonance by comparison to DEA to gas-^{72,73} and condensed-phase⁷⁴ methanol as well as that from amorphous water.⁵⁹ In gas-phase measurements of DEA to methanol, three well-defined maxima are observed. The first and second peaks appear at incident electron energies of 6.5 and 8.0 eV, respectively, with an energetic threshold near 5 eV; they were assigned^{72,75} to the long-lived Feshbach resonances $^2A''[(\text{core})(2a'')^1(3sa'')^2]$ and $^2A'[(\text{core})(7a')^1(3sa')^2]$, respectively, with corresponding parent Rydberg states $^{1,3}A''$ and $^{1,3}A'$. The third resonance was observed at 10.5 eV. These first two peaks were found to arise exclusively from bond cleavage of the hydroxyl group, whereas the last peak was found to originate from both the hydroxyl and methyl groups via a rearranged anionic complex. In contrast, H^- yield functions from multilayer films of methanol showed that while OH bond cleavage was primarily responsible for the H^- ESD signal below 9 eV, a contribution to the H^- signal above this energy was found also to arise from CH dissociation. A maximum at 8.7 eV and a shoulder near 7.3 eV were assigned to the $^2A''$ and $^2A'$ anion configurations.

These results strongly suggest that the 7.3 eV feature in **II** arises from a dissociative mechanism similar to that observed in methanol, i.e., dissociation of the hydroxyl O–H bond. The fact that it appears at the same energy as in the latter is not surprising, since for methanol and higher alcohols the 3s Rydberg band appears at nearly identical energies.^{70,71} As the alkyl group increases in size, the oxygen 3s orbital becomes more delocalized over the alkyl group and the 3s term value decreases.^{70,71} Consequently, the band position remains nearly constant with increasing group size.

We also expect to see a second broad band superimposed on the 10 eV H^- signal near 8.7. However, in the gas phase, the DEA signal from methanol near 8 eV appears much weaker than the lower energy one. Thus, in the present measurement, this peak is likely to be buried under the large intensity H^- signal at 10 eV, but the small shoulder near 8.7 eV in **II** of Figure 2 may indeed correspond to the $^2A'$ Feshbach resonance.

The apparent lack of equivalent Feshbach resonances in the H^- ESD yield curve for **III** is puzzling. Considering the similarity of the CH_2OH moiety to that of methanol and the lower 10 eV H^- signal, we should expect the OH resonances to be more pronounced than for **II**. We do note, however, an increased width in the 10 eV H^- peak toward low energies and

the weak structure near $E_i = 7.3$ eV, suggesting that a Feshbach resonance below 8 eV contributes to the DEA signal.

A search for larger mass fragments desorbing from the surface, such as the $(M - 1)^-$ ion in **I**, **II**, and **III**, or OH^- and CH_2OH^- negative ions in **II** and **III**, yielded negative results; i.e., no ESD signal was detected for any of these larger mass fragments under the same conditions of current and accumulation time. This, however, does not preclude the possibility of larger negative ion fragments forming in the bulk or at the surface of the film. Resonant dissociative attachment of electrons to furan ($\text{C}_4\text{H}_4\text{O}$) in the gas phase,^{45,46} for example, reveal three possible resonances in the $(M - 1)^-$ negative ion yield with energy maxima located at 3.5, 5.55, and 9.8 eV. Other examples for cyclic hydrocarbons, i.e., benzene, show that in the gas phase the $\text{C}_6\text{H}_5^- + \text{H}^\bullet$ DEA channel dominates,^{73,76} whereas in the condensed phase the $\text{H}^- + \text{C}_6\text{H}_5^\bullet$ channel is the only observable one in ESD measurements.¹² It therefore seems likely that for **I**, **II**, and **III** similar $(M - 1)^-$ fragments, as well as other high-mass anionic fragments, are formed upon electron capture but because of the higher mass of these fragments, they do not possess sufficient KE to escape the polarization potential, E_p , of the dielectric film.

The latter is attributed to image-charge-induced polarization interactions of neighboring molecules with the anion formation site and thus provides an energetic barrier that a desorbing anion must overcome.^{22,61,75} Therefore, if the E_k of the anion fragment is less than E_p , it will become trapped in the film where it may undergo various postdissociation reactions.¹¹ However, if the anionic fragments possess sufficient KE to overcome E_p , they may desorb or suffer energy losses by elastic or inelastic scattering in the film with or without prior refraction. In the latter case they may either become trapped in the film or desorb with lowered E_k . Thus, the effect of E_p is twofold. It lowers the NIS energy relative to that of the neutral ground state, but the limit it imposes for the stable anion fragment to escape the film causes a shift to higher incident energies of the anion desorption threshold and maximum intensity. The combined effect depends also on the energy and shape of the anion potential energy surface. The polarization shift of the NIS to lower energies is usually on the order of 1 eV.

To estimate the effects of E_p on H^- desorption yields from **I**, **II**, and **III**, as well as the effects of electron energy losses prior to DEA and collisional ion energy losses in the solid prior to desorption, we have measured H^- kinetic energy distributions and HREEL spectra at selected incident electron energies. These are presented and discussed in the following two sections.

B. H^- Kinetic Energy Distributions. KE distributions of H^- were measured at an incident energy of 10 eV from 10 ML thick films of **I**, **II**, and **III**. The choice of E_i is such that it corresponds to the maximum in the H^- DEA peak. Shown in Figure 3 is the first negative energy derivative of the retardation curves as discussed in section II. Vertical arrows indicate $E_k(\text{mp})$ and $E_k(\text{max})$. The KE distributions are peaked at approximately 0, 1.1, and 0.9 eV, with an $E_k(\text{max})$ at 4.1, 4.8, and 4.3 eV for **I**, **II**, and **III**, respectively.

The E_k of H^- , after desorption, can be written as⁵⁸

$$E_k(\text{H}^-) = (1 - \beta)[E_i - \Delta E_i - (D_0 - A_e) - E^* + E_p] - [E_p + \Delta E_{\text{H}}] \quad (1)$$

Here, β is the mass ratio of the anion fragment H^- to that of the neutral parent molecule, E_i the incident electron energy, D_0 the energy required for homolytic bond cleavage along the dissociation coordinate, A_e the electron affinity of hydrogen

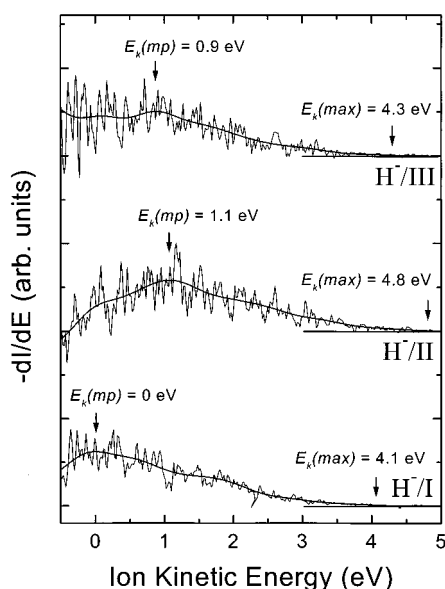


Figure 3. H^- kinetic energy distributions for **I**, **II**, and **III** measured for incident electron energies $E_i = 10$ eV. Indicated in this figure are the approximate positions of the most probable energy $E_k(\text{mp})$ and the maximum energy $E_k(\text{max})$. The smooth solid lines serve as guides to the eye, and the curve baselines have been shifted vertically for clarity.

(0.75 eV²⁰), and E^* the total internal energy of the neutral fragment, or fragments, after dissociation. Condensed-phase effects such as the solid's average polarization energy, electron energy losses prior to DEA, and collisional energy losses prior to desorption, any combination of which can contribute to the final KE of the desorbed anion, are contained in the first and second terms of eq 1 and are represented by, respectively, E_p , ΔE_i , and ΔE_H .⁷⁷ From the β term it is apparent that light fragments, which contain more KE, are more likely to escape the polarization force induced by the anion, whereas heavier fragments are more likely to remain trapped in the bulk or at the surface of the film, even if the dissociation event favors formation of heavier fragments. Owing to the small relative mass of H^- produced via DEA to **I**, **II**, and **III**, for which $\beta \leq 0.014$, E_p in the first and second terms may be eliminated. In this case, eq 1 can be approximated as⁷⁸

$$E_k(\text{H}^-) \approx [E_i - (D_0 - A_e) - E^*] - [\Delta E_i + \Delta E_H] \quad (2)$$

The first term in eq 2 represents the minimal thermodynamic relationship, which must always apply, and is equivalent to the maximum H^- KE that would be allowed in the gas phase at low pressures.

Hence, by neglecting the effects of ΔE_i and ΔE_H , we may, from the first term in eq 2, calculate the largest possible allowed value of E_k given the bond dissociation energy, D_0 , and electron affinity, A_e , of the atomic hydrogen fragment. If we assume the primary dissociation channel that produces H^- ion arises from cleavage of an endocyclic $\alpha\text{-C-H}$ bond ($D_0 \cong 4.0$ eV,^{65,79} $A_e(\text{H}) = 0.75$ eV), the maximum possible KE values, assuming $E^* = 0$ eV, for **I**, **II**, and **III** from eq 2 will be identical and are estimated at 6.75 eV. The $E_k(\text{max})$ values determined from retardation curves and indicated in Figure 3, on the other hand, are 4.1, 4.8, and 4.3 eV, respectively, for **I**, **II**, and **III**. The calculated $E_k(\text{max})$ values are in excess of those measured by 2.65, 1.95, and 2.45 eV, respectively, and therefore must correspond to E^* of the neutral DEA fragment(s), i.e., highly vibrationally excited neutrals. At first, these values for E^* would appear to be unreasonable. However, given an initial electron

attachment energy within the Franck–Condon region and the short dissociation times involved, it may be possible to obtain such highly excited neutral fragments if the initial excitation leads to bond cleavage within the lifetime of the NIS as discussed below.

We consider that the initial excitation in the core-excited shape resonance responsible for the 10 eV H^- production via DEA is that of an oxygen lone pair electron. Thus, since the weakest bond in **I** is the C–O bond ($D_0 = 3.69$ eV⁸⁰) the initial excitation may promote CO bond cleavage.^{38–44} The photochemical reaction dynamics of cyclic ethers, in particular the cleavage reactions in **I**,^{38–44} are fairly well characterized. Gas-, liquid-, and solid-phase photolyses of **I** demonstrate that upon excitation a photoinduced ring-opened oxyl alkyl diradical transient is formed. More importantly, Scala et al.⁴⁴ have recently reported that the lifetime of the transient neutral **I** is $\sim 6.5 \times 10^{-14}$ s; that is, α -cleavage of the C–O bond in **I** occurs within this lifetime. Thus, conceivably, CO bond cleavage within the lifetime of the NIS may indeed be possible if the lifetime of the NIS is at least on the order of the time necessary for C–O bond rupture, i.e., 6.5×10^{-14} s. Therefore, following nonconcerted dissociation of the adjacent $\alpha\text{-CH}$ bond, the α -cleaved diradical is left in a vibrationally excited state whose energy will depend on the excitation energy minus the C–O and C–H bond dissociation energies plus the release of ring strain (~ 0.3 eV⁷⁹). Since 65 fs is too short a time to allow appreciable vibrational thermalization, the upper limit estimate of ~ 2.61 eV for E^* , given an incident electron energy of 10 eV, is expected to be released into vibrational excitation. This value is in excellent agreement with the value of 2.65 eV determined for E^* using eq 2. If the assumption of rapid C–O bond cleavage within the lifetime of the NIS is valid, it could account for the excess internal energy in the neutral DEA fragment. Evidence of the formation of products or fragments resulting from α -cleavage of solid **I** under electron impact has been found here in electronic excitation HREEL measurements and will be discussed in the following section.

For ions produced in the solid state, $E_k(\text{mp})$ may include condensed-phase effects such as EEL prior to DEA, and collisional ion energy loss in the solid prior to desorption, such that the in vacuo $E_k(\text{max})$ may be lowered by any one of these processes. Thus, the effect of the second term in eq 2, $\Delta E_i + \Delta E_H$, must account for the KE difference between $E_k(\text{max})$ and $E_k(\text{mp})$ of the H^- ion. For **I**, **II**, and **III**, this amounts to about 4.1, 3.7, and 3.4 eV, respectively. At 10 eV incident energy, however, electronic excitation prior to DEA would reduce E_i to energies below those necessary to access the NIS, whereas vibrational and phonon excitations would contribute to energy transfers of about 0.1–0.5 eV for the present film thickness.⁸¹ Thus, the KE difference between $E_k(\text{mp})$ and $E_k(\text{max})$ is essentially attributable to *postdissociative* collisional losses due to anion scattering within the film. In Figure 3, the near-thermal $E_k(\text{mp})$, coupled with the high-energy tail extending to ~ 4 eV seen in the H^- KE distributions from solid **I**, is therefore indicative of a large degree of elastic and inelastic anion scattering at or near the surface prior to desorption. Similarly, the low-energy tail and broad features seen in the H^- KE distributions from solids **II** and **III** suggest that ion scattering plays a significant role. Excess internal energy in the neutral ring fragment(s) in the latter, however, would necessarily lead to more vibrational excitation in the neutral fragment, since more internal degrees of freedom are available for excitation than in the exocyclic moieties.

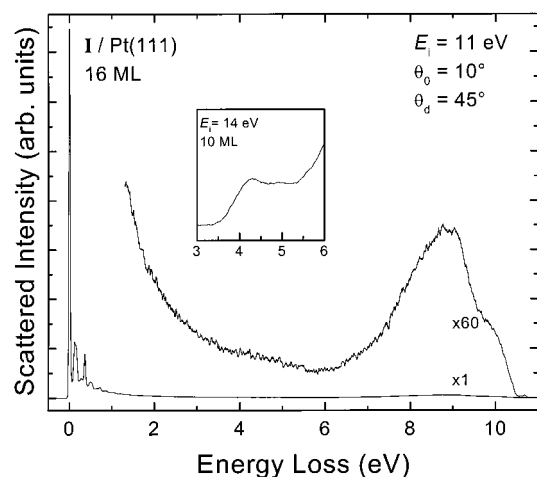


Figure 4. High-resolution electron energy loss (HREEL) spectrum measured from a 16 ML film of **I** deposited on a Pt(111) crystal at an E_i of 11 eV and an incident θ_0 and collection angle θ_d of 10° and 45° , respectively. Inset: HREEL spectrum of a 10 ML film of **I** measured at an E_i of 14 eV. θ_0 and θ_d were set at 10° and 45° , respectively.

C. Electron Energy Loss. Figure 4 shows the HREEL spectrum from a 16 ML film of **I** condensed at ~ 24 K; it was recorded with an incident electron energy (E_i) of 11 eV and incident and deflection angles of 10° and 45° , respectively. An incident energy of 11 eV was chosen such that it lies within the energy range of the 10 eV negative ion resonance, while simultaneously maintaining constant transmission down to 1 eV residual energy in the zoom lens of the analyzer. The peak near 0 eV corresponds to elastically and quasi-elastically scattered electrons followed by excitation of vibrational and combination modes extending to approximately 1 eV. A detailed analysis⁵⁷ of vibrational excitation functions showed that the intensities of the vibrational modes in solid **I** are governed by electron resonances and that at least three of them are responsible for enhancing the vibrational excitation cross sections. Between 1 and 6 eV the spectrum is dominated by multiple phonon and vibrational inelastic losses. The feature beginning near 6 eV and having a maximum near 8.7 eV is attributed to the excitation of several overlapping electronic states in solid **I**. The shoulder peak seen at 10 eV in Figure 4 was also observed at the same residual energy for different E_i and therefore is not attributed to electronic excitation.

The diffuse nature of the electronic bands makes the spectrum in Figure 4 difficult to interpret, but similarities exist in comparison to both the near-threshold gas-phase EEL spectrum of Bremner et al.⁵² and VUV^{52,54–56} spectra. The very weak band near threshold reaches a maximum near 6.66 eV. The peak correlates well with the lowest observed electronic state in gaseous **I** located at 6.6 eV in VUV spectra^{52,54–56} and is attributed to the lowest Rydberg state n_03s . In the gas-phase EEL spectrum⁵² of **I** the first optically allowed transition has its maximum at ~ 6.4 eV, an energetic threshold near 5.6 eV, and extends to ~ 6.8 eV and is believed to incorporate mixed valence and Rydberg states as well as the lowest 3n_03s state. A second weak shoulder peak near 7.8 eV is seen in Figure 4 and may correlate with the n_03p state at 7.2 eV observed in the VUV spectra or between 7.4 and 7.6 eV in gas-phase EELS spectra. Above this energy we are no longer able to resolve any additional bands that may be attributable to the higher np Rydberg series. This is to be expected, since the bands seen above 8 eV in VUV spectra of gaseous **I** are highly Rydberg in character and are expected to become more diffuse upon condensation and be strongly shifted up in energy.⁷⁰ Finally,

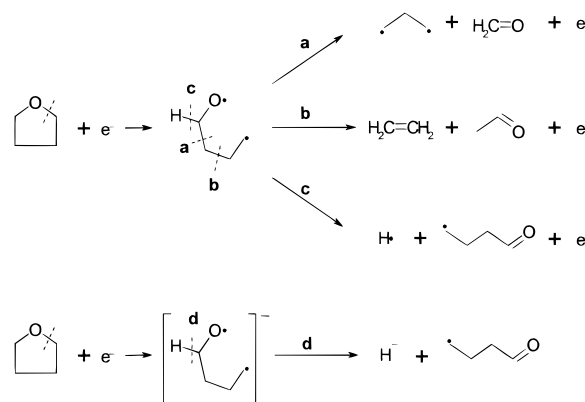


Figure 5. Scheme showing the relevant reactions leading to the formation of small CO π -bonded products.

the peak maximum at 8.7 eV would appear to correlate best with the n_04p state at 8.57 eV in the VUV spectrum. However, given the above consideration, it seems more likely that this peak corresponds to the 1n_03s ($HOMO-1 \rightarrow 3s$) transition observed near 8.1 eV in VUV spectra^{52,54–56,70} of gaseous **I**.

Shown in the inset of Figure 4 is an expanded view of the energy-loss region between 3 and 6 eV, measured from a 10 ML film of **I** bombarded with the electron beam ($I_0 = 0.1$ nA, $E_i = 14$ eV) for 60 min. For such long exposures to the beam, a maximum in the signal is observed at ~ 4.25 eV. The observed energy loss peak near 4.25 eV cannot be accounted for by excitation of a singlet (or triplet) state in **I**, even after taking into consideration condensation effects such as hydrogen bonding, which can lower the ground-state energy by 0.2–0.5 eV.⁸² Although the lowest triplet state in **I** has not been conclusively identified, it is proposed⁵² to reside near the lowest optically allowed singlet state at 6.6 eV. Excluding these transitions as the origin of the 4.25 eV structure, we are left to consider that the 4.25 eV loss peak is due to excitation of a degradation product or fragment resulting from previous electron bombardment. The association of this peak with the formation of degradation products is further established by electron dose response measurements. In a series of energy loss spectra, recorded at $E_i = 14$ eV over the low-energy excitation region as a function of electron bombardment time (10–60 min), it was found that for each subsequent scan the 4.25 eV energy loss peak gained intensity. In addition, it was confirmed that the intensity gain was not due to film charging effects or that the structure was due to an impurity.⁵⁷ Thus, we believe that this structure is due to electronic excitation of a degradation product. We propose that the 3.5–5 eV signal arises from a weak $n-\pi^*$ transition (R band) in formaldehyde, acetaldehyde, and/or *n*-butyraldehyde, which are expected to be formed by a dissociative resonant or a direct nonresonant electron scattering process. We cannot, however, completely exclude the possibility that furan, which may be formed following H^- elimination after DEA or following elimination of neutral H, could also contribute to the 4 eV signal. On the basis of a comparison of previous experimental^{83–87} and theoretical^{88–90} work, we conclude that the neutral H or H^- elimination reactions leading to the formation of furan are not likely to occur and therefore are not considered here. As a final test, a residual gas analysis of **I** prior to deposition confirmed the sample purity, i.e., that the sample was not contaminated with furan, dihydrofuran, or any of the above-mentioned carbonyl-containing compounds.

In Figure 5, we show the relevant reactions leading to the formation of C–O π -bonded products, which are likely to be responsible for the 4.25 eV loss peak. All four reactions a–d

are energetically accessible upon excitation of **I** by either a resonant or nonresonant mechanism. Several possible reaction channels are available: disproportionation reactions a and b of the transient intermediate into smaller C–C and C–O π -bonded products such as ethylene and formaldehyde, elimination reaction c of neutral H from the ring-opened intermediate, and H[−] elimination reaction d following DEA. The lack of an H[−] signal at 14 eV in ESD suggests that H[−] is not produced by $E_i = 14$ eV electrons used to record the HREEL data in the inset of Figure 4. Thus, we consider neutral H elimination or disproportionation yielding large and small carbonyl-containing fragments, (reactions a–c) via a direct or resonant electronic excitation process. Condensed-phase UV photolysis studies⁴³ of the fragmentation pathways in **I** find β -cleavage of the initially formed oxyl alkyl diradical to be a major dissociation channel and that C–O π bond products are favored over C–C π bond products. Secondary dissociation channels leading to the formation of smaller neutral fragments such as CO and methylene are found to occur in the solid state but to a lesser extent than in gas-phase photolysis of **I**. We have confirmed that CO is not produced by electron bombardment of solid **I**, and therefore, secondary dissociation reactions of the transient diradical is not expected to be a major competing fragmentation pathway. This supports interpretation of the 4.25 eV peak in Figure 4 as due to excitation of a carbonyl chromophore attributed to *n*-butyraldehyde (c), acetaldehyde (b), or formaldehyde (a), where the last two are expected from condensed-phase UV photolysis. Unfortunately, we are not able to distinguish between the different carbonyl compounds in the present experiments owing to the nearly identical excitation energy of the different carbonyl chromophores; additional experimental evidence, such as formation of CO or bands attributable to CC π -bonded products, is also lacking.

UV absorption spectra locate the $n-\pi^*$ transition in formaldehyde and acetaldehyde in aqueous solution at 4.41 and 4.52 eV, whereas in nonpolar hexane solution they shift to 4.23 and 4.23 eV, respectively.⁹¹ Similarly, UV absorption spectra of *n*-butyraldehyde measured in the gas⁹² and liquid^{91,93–95} phase locate a weak $n-\pi^*$ transition at 4.23 and 4.35 eV, respectively. The observed blue shift in aqueous solution is attributed to a net stabilization of the ground electronic state in water, which is not expected to affect the less polar carbonyl excited state.^{93,96} In nonpolar hexane solution the absorption maximum is found to be 4.23 eV.⁹¹ Low-energy electron impact excitation spectra of formaldehyde and acetaldehyde in the gas phase, however, places the lowest $^3,^1n\pi^*$ states at 3.80 and 3.91 eV, respectively.⁹⁷ If this trend continues with increasing chain length, then *n*-butyraldehyde might be expected to have an electron impact induced excitation at or near 4.2 eV. Thus, in the absence of additional experimental evidence to the contrary, we favor reaction c.

IV. Summary and Conclusions

Via anion ESD and HREEL spectroscopy, we have examined the low-energy electron-induced degradation of a series of model compounds condensed at 27 K on polycrystalline Pt, which are representative of the deoxyribose backbone in DNA. In each of these, i.e., tetrahydrofuran (**I**), 3-hydroxytetrahydrofuran (**II**), and α -tetrahydrofurfuryl alcohol (**III**), we find only H[−] desorbing from the surface, but experimental HREEL measurements suggest that the dissociation channels in at least **I** may be more complex. For each of the three species, we further find that the 10 eV H[−] ESD yield arises from selective dissociation of the α -C–H bonds. In addition to the 10 eV ESD peak in **II**, we find a second lower energy resonance near 7.3 eV that

correlates well with the Feshbach resonance observed in solid methanol, though a similar Feshbach resonance in the H[−] ESD yield from **III** is not apparent.

A search of the electronic excitation region of condensed thick films of **I** using the HREEL technique revealed a broad, featureless excitation extending from 6 to 10 eV energy loss, with a peak maximum centered near 8.7 eV, which is attributed to excitation of several overlapping electronic states. We propose that the parent NIS at ~ 10 eV has its origin in a lower-lying σ - or n -type MO; i.e., electron promotion originates from an MO below that of the HOMO or HOMO-1 and that this 10 eV DEA peak may correspond to one or more dissociative core-excited shape resonances. In addition, on the basis of the relatively high value for E^* , determined using eq 2 and the experimental value for $E_k(\text{max})$, we propose that during the lifetime of the NIS, α -cleavage of the C–O bond also occurs. The complexity of the dissociation mechanisms within the condensed solid **I** is further revealed by the observation of a unique energy loss feature appearing at ~ 4.25 eV in the HREEL spectrum measured, at an E_i of 14 eV, which is attributed to excitation in *n*-butyraldehyde produced via a ring-opened transient neutral intermediate. This conclusion is supported on the basis of a comparison with photofragmentation studies of **I** in the gas, liquid, and solid phases.

On the basis of our present experimental results, we propose that an attack of the deoxyribose backbone in cellular DNA by 6–14 eV secondary electrons is likely to lead to strand lesions via either DEA to exocyclic groups or resonance-enhanced cleavage of ring bonds (Figure 5), where the latter results in a complete dissociation of the sugar. Subsequent reactions of the energetic anions [$E_k(\text{max}) \approx 4.5$ eV], or radical aldehyde-type fragments, with an adjacent phosphate or base will further promote the formation of a multiply damaged site in cellular DNA. Although the present results do not provide a scenario of cellular radiolysis of DNA, they do represent a model system with respect to the radiobiological action of low-energy secondary electrons. Thus, we believe that detailed investigations into the nature of low-energy resonant electron interactions with biologically relevant molecules warrant further efforts and will unquestionably contribute to a better understanding of the pernicious, as well as beneficial, effects of ionizing radiation.

Acknowledgment. D.A. acknowledges the support of the Gouvernement du Québec, Ministère de l'Éducation, in the form of a postdoctoral fellowship (Program Québécois de Bourse d'Excellence). D.A. also thanks Dr. Michael Huels for his unending patience during the preparation of this manuscript and also for many helpful discussions and comments. This research is supported by the Medical Research Council of Canada.

References and Notes

- Sanche, L. *IEEE Trans. Electr. Insul.* **1993**, 28, 789–819.
- Bass, A. D.; Cloutier, P.; Sanche, L. *J. Appl. Phys.* **1998**, 84, 2740–2748.
- Rowntree, P.; Dugal, P. C.; Hunting, D.; Sanche, L. *J. Phys. Chem.* **1996**, 100, 4546–4550.
- Olsen, C.; Rowntree, P. *J. Chem. Phys.* **1998**, 108, 3750–3764.
- Klyachko, D.; Rowntree, P.; Sanche, L. *Surf. Sci.* **1996**, 346, L49–L54.
- Di, W.; Rowntree, P.; Sanche, L. *Phys. Rev. B* **1995**, 52, 16618–16622.
- Martel, R.; Avouris, P.; Lyo, I.-W. *Science* **1996**, 272, 385–388.
- Sambe, H.; Ramaker, D. E.; Deschênes, M.; Bass, A. D.; Sanche, L. *Phys. Rev. Lett.* **1990**, 64, 523–526.
- Sanche, L.; Bass, A. D.; Ayotte, P.; Fabrikant, I. I. *Phys. Rev. Lett.* **1995**, 75, 3568–3571.
- Ayotte, P.; Gamache, J.; Bass, A. D.; Fabrikant, I. I.; Sanche, L. *J. Chem. Phys.* **1997**, 106, 749–760.
- Huels, M. A.; Parenteau, L.; Sanche, L. *J. Chem. Phys.* **1994**, 100, 3940–3956.

- (12) Rowntree, P.; Sambe, H.; Parenteau, L.; Sanche, L. *Phys. Rev. B* **1993**, *47*, 4537–4554.
- (13) Sanche, L. *Scanning Microsc.* **1995**, *9*, 619–656.
- (14) Huels, M. A.; Khoury, J.; Gueraud, B.; Boudaiffa, B.; Dugal, P. C.; Hunting, D.; Sanche, L. In *Microdosimetry: An Interdisciplinary Approach*; Goodhead, D. T., O'Neill, P., Menzel, H. G., Eds.; The Royal Society of Chemistry Press: Cambridge, U.K., 1997; pp 89–92.
- (15) ICRU Report 31, International Commission on Radiation Units and Measurements, Washington, DC, 1979.
- (16) Pimlott, S. M.; LaVerne, J. A. In *Radiation Damage in DNA: Structure/Function Relationships at Early Times*; Fuciarelli, A. F., Zimbrick, J. D., Eds.; Battelle Press: Columbus, OH, 1995; pp 3–12.
- (17) Cobut, V.; Frongillo, Y.; Patau, J. P.; Goulet, T.; Fraser, M.-J.; Jay-Gerin, J.-P. *Radiat. Phys. Chem.* **1998**, *51*, 229–243.
- (18) Frongillo, Y.; Goulet, T.; Fraser, M.-J.; Cobut, V.; Patau, J. P.; Jay-Gerin, J.-P. *Radiat. Phys. Chem.* **1998**, *51*, 245–254.
- (19) Sanche, L. *Radiat. Phys. Chem.* **1989**, *34*, 15–33.
- (20) Christophorou, L. G. *Atomic and Molecular Radiation Physics*; Wiley-Interscience: London, 1971; p 546.
- (21) Illenberger, E. In *Gaseous Molecular Ions: An Introduction to Elementary Processes Induced by Ionization*; Baumgärtl, H., Frank, E. U., Grünbein, W., Eds.; Steinkopff Verlag Darmstadt Springer-Verlag: New York, 1992; pp 241–337.
- (22) Rowntree, P.; Parenteau, L.; Sanche, L. *J. Phys. Chem.* **1991**, *95*, 4902–4909.
- (23) Huels, M. A.; Parenteau, L.; Sanche, L. To be published.
- (24) Huels, M. A.; Parenteau, L.; Sanche, L. *Chem. Phys. Lett.* **1997**, *279*, 223–229.
- (25) Dugal, P. C.; Huels, M. A.; Sanche, L. *Radiat. Res.* **1999**, *151*, 325–333.
- (26) Huels, M. A.; Hahndorf, I.; Illenberger, E.; Sanche, L. *J. Chem. Phys.* **1998**, *108*, 1309–1312.
- (27) Huels, M. A.; Herve du Penhoat, M. A.; Cloutier, P.; Khoury, J.; Jay-Gerin, J.-P.; Sanche, L. To be published.
- (28) Klyachko, D. V.; Huels, M. A.; Sanche, L. *Radiat. Res.* **1999**, *151*, 177–187.
- (29) Colson, A.-D.; Sevilla, M. D. *J. Phys. Chem.* **1995**, *99*, 3867–3874.
- (30) Colson, A.-D.; Sevilla, M. D. *Int. J. Radiat. Biol.* **1995**, *67*, 627–645.
- (31) Close, D. M. *Radiat. Res.* **1997**, *147*, 663–673.
- (32) Yan, M.; Becker, D.; Summerfield, S. R.; Renke, P.; Sevilla, M. D. *J. Phys. Chem.* **1992**, *96*, 1983–1989.
- (33) Bernhard, W. A. *J. Phys. Chem.* **1989**, *93*, 2187–2189.
- (34) Sevilla, M. D.; Becker, D.; Yan, M.; Summerfield, S. R. *J. Phys. Chem.* **1991**, *95*, 3409–3415.
- (35) Cullis, P. M. *J. Chem. Soc., Perkin Trans. 2* **1992**, 1695–1702.
- (36) Swarts, S. G.; Becker, D.; Sevilla, M. D.; Wheeler, K. T. *Radiat. Res.* **1996**, *145*, 304–314.
- (37) Margerum, J. D.; Pitts, J. N.; Rutgers, J. G.; Searles, S. J. *Am. Chem. Soc.* **1959**, *81*, 1549–1554.
- (38) Roquette, B. C. *J. Phys. Chem.* **1966**, *70*, 1334–1335.
- (39) Roquette, B. C. *J. Am. Chem. Soc.* **1969**, *91*, 7664–7667.
- (40) Kizilkilic, N.; Schuchmann, H.-P.; von Sonntag, C. *Can. J. Chem.* **1980**, *58*, 2819–2826.
- (41) von Sonntag, C. *Photophysics and Photochemistry in the Vacuum Ultraviolet*; McGlynn, S. P., Findley, G. L., Huebner, R. H., Eds.; Reidel: Dordrecht, 1985; pp 913, 927.
- (42) Diaz, Z.; Doecker, R. D. *J. Phys. Chem.* **1978**, *82*, 10–14.
- (43) Scala, A. A.; Rourke, W. J. *J. Photochem.* **1987**, *37*, 281–292.
- (44) Scala, A. A.; Diau, E. W.-G.; Kim, Z. H.; Zewail, A. H. *J. Chem. Phys.* **1998**, *108*, 7933–7936.
- (45) Muftakhov, M. V.; Asfandiarov, N. L.; Khvostenko, V. I. *J. Electron Spectrosc. Relat. Phenom.* **1994**, *69*, 165–175.
- (46) Khvostenko, V. I.; Vorob'yov, A. S.; Khvostenko, O. G. *J. Phys. B: At. Mol. Opt. Phys.* **1990**, *23*, 1975–1977.
- (47) Khvostenko, O. G.; Zykov, B. G.; Asfandiarov, N. L.; Khvostenko, V. I.; Denisenko, S. N.; Shustov, V. G.; Kostyanovsky, R. G. *Khim. Fiz. SSSR* **1985**, *4*, 1336–1373.
- (48) Khvostenko, V. I.; Khvostenko, O. G.; Asfandiarov, N. L.; Tolstikov, G. A. *Dokl. Akad. Nauk SSSR* **1986**, *291*, 1172–1177.
- (49) Colson, A.-D.; Besler, B.; Sevilla, M. D. *J. Phys. Chem.* **1993**, *97*, 8092–8097.
- (50) Tasaki, K.; Yang, X.; Urano, S.; Fetzer, S.; LeBreton, P. R. *J. Am. Chem. Soc.* **1990**, *112*, 538–548.
- (51) Miaskiewicz, K.; Osman, R. J. *Am. Chem. Soc.* **1994**, *116*, 232–238.
- (52) Bremner, L. J.; Curtis, M. G.; Walker, I. C. *J. Chem. Soc., Faraday Trans.* **1991**, *87*, 1049–1055.
- (53) Tam, W.-C.; Brion, C. E. *J. Electron Spectrosc. Relat. Phenom.* **1974**, *3*, 263–279.
- (54) Davidson, R.; Høg, J.; Warsop, P. A.; Whiteside, A. B. *J. Chem. Soc., Faraday Trans. 2* **1972**, *68*, 1652–1658.
- (55) Doucet, J.; Sauvageau, P.; Sandorfy, C. *Chem. Phys. Lett.* **1972**, *17*, 316–319.
- (56) Pickett, L. W.; Hoeflich, N.; Liu, T.-C. *J. Am. Chem. Soc.* **1951**, *73*, 4865–4869.
- (57) Lepage, M.; Letarte, S.; Michaud, M.; Motte-Tollet, F.; Hubin-Frankin, M.-J.; Roy, D.; Sanche, L. *J. Chem. Phys.* **1998**, *109*, 5980–5986.
- (58) Huels, M. A.; Parenteau, L.; Michaud, M.; Sanche, L. *Phys. Rev. A* **1995**, *51*, 337–349.
- (59) Rowntree, P.; Parenteau, L.; Sanche, L. *J. Chem. Phys.* **1991**, *94*, 8570–8576.
- (60) Sanche, L.; Deschênes, M. *Phys. Rev. Lett.* **1988**, *61*, 2096–2098.
- (61) Sanche, L.; Michaud, M. *Phys. Rev. B* **1984**, *30*, 6078–6092.
- (62) Michaud, M.; Cloutier, P.; Sanche, L. *Rev. Sci. Instrum.* **1995**, *66*, 2661–2667.
- (63) Sanche, L. *J. Chem. Phys.* **1979**, *71*, 4860–4882.
- (64) Antic, D.; Parenteau, L.; Sanche, L. To be published.
- (65) Golden, D. M.; Benson, S. W. *Chem. Rev.* **1969**, *69*, 125–134.
- (66) Weast, R. C., Ed. *CRC Handbook of Chemistry and Physics*, 72nd ed.; CRC Press: Boca Raton, FL, 1991.
- (67) The structures investigated in these theoretical studies are (R)-amino-(S)-4-hydroxy-5-methyltetrahydrofuran, 2'-deoxyribose-3',5'-biphosphate, and 2'-deoxyribose-1'-amino-3',5'-biphosphate. While there are structural similarities to the model compounds studied here, caution should be used in making a direct comparison to these theoretical results, since the degree of substitution in the former may result in larger distortions in the geometry-optimized structures.
- (68) Allan, M.; Andric, L. *J. Chem. Phys.* **1996**, *105*, 3559–3568.
- (69) Sanche, L.; Schulz, G. J. *J. Chem. Phys.* **1973**, *58*, 479–493.
- (70) Robin, M. B. *Higher Excited States of Polyatomic Molecules*; Academic Press: New York, 1974; Vol. III.
- (71) Robin, M. B. *Higher Excited States of Polyatomic Molecules*; Academic Press: New York, 1974; Vol. I.
- (72) Curtis, M. G.; Walker, I. C. *J. Chem. Soc., Faraday Trans.* **1992**, *88*, 2805–2810.
- (73) von Trepka, L.; Neuert, H. Z. *Naturforsch. A* **1963**, *18*, 1295–1303.
- (74) Parenteau, L.; Jay-Gerin, J.-P.; Sanche, L. *J. Phys. Chem.* **1994**, *98*, 10277–10281.
- (75) Michaud, M.; Fraser, M.-J.; Sanche, L. *J. Chim. Phys.* **1994**, *91*, 1223–1227.
- (76) Fenzlaff, H.-P.; Illeberger, E. *Int. J. Mass. Spectrom. Ion Processes* **1984**, *59*, 185–202.
- (77) Huels, M. A.; Parenteau, L.; Sanche, L. *Phys. Rev. B* **1995**, *52*, 11343–11350.
- (78) For H^+ produced via DEA to large mass molecules the $(1 - \beta)$ term in eq 2 is close to unity. In the case of H^+ production from **I**, **II**, and **III** β is 0.014, 0.011, and 0.098, respectively, which yields a $(1 - \beta)$ of ≥ 0.986 . Thus, the contribution E_p to the in vacuo E_k is negligible, since $(1 - \beta)E_p - E_p \approx 0$.
- (79) Lowry, T. H.; Richardson, K. S. *Mechanisms and Theory in Organic Chemistry*, 3rd ed.; Harper Collins: New York, 1987; pp 161–162.
- (80) Green, J. H. S. *Q. Rev., Chem. Soc.* **1961**, *15*, 125–152.
- (81) Michaud, M.; Sanche, L. *Phys. Rev. Lett.* **1987**, *59*, 645–648.
- (82) Dressler, K.; Schnepf, O. *J. Chem. Phys.* **1960**, *33*, 270–274.
- (83) Flicker, W. M.; Mosher, O. A.; Kuppermann, A. *Chem. Phys. Lett.* **1976**, *38*, 489–492.
- (84) Palmer, M. H.; Walker, I. C.; Ballard, C. C.; Guest, M. F. *Chem. Phys.* **1995**, *192*, 111–125.
- (85) van Veen, E. H. *Chem. Phys. Lett.* **1976**, *41*, 535–539.
- (86) Flicker, W. M.; Mosher, O. A.; Kuppermann, A. *J. Chem. Phys.* **1976**, *64*, 1315–1321.
- (87) Kuppermann, A.; Flicker, W. M.; Mosher, O. A. *Chem. Rev.* **1979**, *79*, 77–90.
- (88) Thunemann, K.-H.; Buenker, R. J.; Butscher, W. *J. Chem. Phys.* **1980**, *47*, 313–320.
- (89) Nakatsuji, H.; Kitao, O.; Yonezawa, T. *J. Chem. Phys.* **1985**, *83*, 723–734.
- (90) Serrano-Andrés, L.; Merchán, M.; Nebot-Gil, I.; Roos, B. O.; Fülcher, M. *J. Am. Chem. Soc.* **1993**, *115*, 6184–6197.
- (91) Lewis, C. A.; Wolfenden, R. *J. Am. Chem. Soc.* **1973**, *95*, 6685–6688.
- (92) Martinez, R. D.; Buitrago, A. A.; Howell, N. W.; Hearn, C. H.; Joens, J. A. *Atmos. Environ.* **1984**, *18*, 2413.
- (93) Xu, H.; Wentworth, P. J.; Howell, N. W.; Joens, J. A. *Spectrochim. Acta A* **1993**, *49*, 1171–1178.
- (94) Ogata, Y.; Kawasaki, A.; Okumura, N. *Tetrahedron* **1966**, *22*, 1731–1739.
- (95) Kurz, J. L. *J. Am. Chem. Soc.* **1967**, *89*, 3524–3527.
- (96) Lee, E. K. C.; Lewis, R. S. *Adv. Photochem.* **1980**, *12*, 1–96.
- (97) van Veen, E. H.; van Dijk, W. L.; Brongersma, H. H. *Chem. Phys.* **1976**, *16*, 337–345.